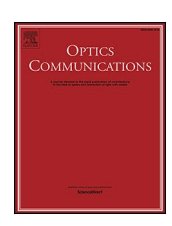
ELSEVIER

Contents lists available at ScienceDirect

# **Optics Communications**

journal homepage: www.elsevier.com/locate/optcom





# Explicit analytic efficiency equation for saturated counter-pumped fiber amplifiers: Application to cladding-pumped erbium-doped fiber amplifiers

Johan Nilsson®

Optoelectronics Research Centre, University of Southampton, Southampton, SO17 1BJ, UK, UK

ARTICLE INFO

Keywords: Modeling Fiber amplifier Optical amplifier Erbium

#### ABSTRACT

We derive and assess an explicit analytic expression for the power conversion efficiency (PCE) of high-power continuous-wave optical fiber amplifiers with counter-propagating pump and signal in the presence of quenching, excited-state absorption, and background loss. The expression is uniquely simple to evaluate. A crucial assumption is that the level populations and thus the gain do not depend on the signal and pump powers separately, but rather on their ratio. In the ideal, "balanced", case, this ratio remains constant throughout the amplifier, which is possible when the signal gain is equal to the operating pump depletion. This is achieved for certain (balanced) combinations of fiber length and input signal and pump power. With these assumptions, the PCE depends only on the spectroscopy and cross-sectional geometry of the gain fiber, but not depend on the absolute power.

We use the equations to calculate and optimize the balanced PCE of homogeneously broadened cladding-pumped  ${\rm Er}^{3+}$ -doped fiber amplifiers based on phosphorus-rich silica fibers. Cases which fulfill as well as deviate from the ideal balanced assumptions are considered. The resulting PCE agrees well with that of well-established numerical simulations in most investigated cases, but agreement gets worse at large deviations from the ideal assumptions. The calculations are sufficiently fast for optimized curves to be updated real-time when parameters (e.g., describing quenching) are changed.

We believe that our approach is valid for a range of realistic systems, including, for example, Yb-doped and Tm-doped fiber amplifiers as well as inhomogeneously broadened systems. We also discuss criteria for the expression's validity and provide tests which are straightforward to evaluate in the balanced case. Validation in more general, "unbalanced" cases, is more difficult and may in many cases require comparisons to iterative numerical simulations.

### 1. Introduction

Rare-earth-doped fiber amplifiers are modeled in a multitude of ways, enabling the calculation of properties such as gain, amplified spontaneous emission (ASE), noise figure, output power, and conversion efficiency (e.g., Refs. [1–4]). These models involve various degrees of sophistication, simplifications, and assumptions, e.g., to treat multiple waveguide modes, bending effects, background loss, quenching, and nonlinearities in a comprehensive or simplified manner. See Ref. [2] for an illustration of some of the effects and assumptions involved with different models. Many models rely on computer simulations with iteration and/or numerical integration of the propagating pump and signal waves, e.g., with a Runge-Kutta algorithm. Other models are simple enough to reduce to an implicit analytic expression [1,2,5–11] (often a

transcendental equation), which can be solved numerically.

For power-scaling through cladding-pumping (e.g., Ref. [12]), the power conversion efficiency (PCE) is particularly important. Cladding-pumping leads to a comparatively low pump intensity with low levels of excitation of the gain medium. For most cladding-pumped fiber amplifiers, the lower laser level (LLL) constitutes the ground state (manifold). For those, stimulated emission typically terminates on a high-lying Stark level with low thermal population in order to reduce reabsorption. In case of a cladding-pumped erbium-doped fiber amplifier (EDFA) operating on the conventional transition between the upper laser level (ULL)  $^4I_{13/2}$  and the ground state  $^4I_{15/2}$ , the emission is therefore at long wavelengths, around 1.6  $\mu$ m (We do not consider Yb-sensitization with energy-transfer [13], which can lead to shorter wavelengths.) Fig. 1 shows a partial energy level diagram including

This article is part of a special issue entitled: Fibres and fibre amplifiers published in Optics Communications. *E-mail address*: jn@orc.soton.ac.uk.

relevant transitions in  ${\rm Er}^{3+}$ , as well as cross-section spectra for transitions involving  $^4I_{13/2}$  and a schematic of the amplifier configuration we consider

Concentration quenching [14–22] limits the  $\rm Er^{3+}$ -concentration. To reach adequate pump absorption, it is therefore necessary to employ long fibers in which the background loss often becomes non-negligible. There is also significant excited-state absorption (ESA) from the ULL at long signal wavelengths [10,21–26]. Background loss, quenching, and ESA all reduce the PCE, so the modeling of cladding-pumped high-power EDFAs should include those effects. This is generally straightforward in numerical simulations, and at least some of them can also be included in implicit analytic expressions [10]. However, we are not aware of any implicit or explicit analytic expression for the PCE when ESA, quenching, and background loss are all significant.

In this paper, we propose and assess a simplified approach leading to a simple explicit expression for the conversion efficiency of continuouswave (cw) optical fiber amplifiers with counter-propagating pump and signal in the presence of quenching, excited-state absorption, and background loss. A crucial assumption is that the gain does not depend on the signal and pump powers separately, but rather on their ratio. This can be the case for a system in which transitions other than those induced by the pump and signal are negligible. Thus, spontaneous emission and amplified spontaneous emission (ASE) are neglected. Another unusual assumption is that the signal gain and operating ("hot") pump depletion are the same. We refer to this as "balanced conditions". When the assumptions are fulfilled, balance can always be realized for appropriate, interlinked, values of signal and pump power, signal gain, pump depletion, and fiber length. Thus, for example, for any combination of input signal and pump power, balance is achieved for a specific fiber length and thus signal gain and pump depletion. We derive equations for a two-level system and use these to calculate the efficiency of cladding-pumped high-power EDFAs in phosphorus-rich erbium-doped silica fibers. We find that the analytically calculated PCE agrees well with the PCE obtained with numerical simulations using established methods in most investigated cases, extending to some cases where the assumptions are not well fulfilled. However, the agreement is worse when the peak gain is so high that ASE becomes significant. We present criteria for the validity of the analytic expressions for the balanced case. Also the criteria can be evaluated non-iteratively. By contrast, when the

assumptions are not well fulfilled (e.g., unbalanced cases), verification may require burdensome comparisons to iterative numerical simulations.

#### 2. Modeling method

Our modeling follows widely used approaches for homogeneously broadened fiber amplifiers (e.g., Refs. [1–4,8,10,27]). Accordingly, the gain per unit length  $g(\lambda, z)$  [Np/m] and evolution of power  $P(\lambda, z)$  at a wavelength  $\lambda$  at the longitudinal fiber position z are given by

$$g\left(\lambda,z\right)=N_{0}\;\Gamma\left(\lambda\right)\left\{ \left[\sigma_{e}\;\left(\lambda\right)-\sigma_{\text{ESA}}\;\left(\lambda\right)\right]n_{2}\;\left(z\right)-\sigma_{a}\;\left(\lambda\right)\;n_{1}\;\left(z\right)\right\} -\alpha_{BG}\;\left(\lambda\right)$$
 Eq. (1)

and

$$dP\left(\lambda,z\right)\ /\ d\left(\pm z\right)=g\left(\lambda,z\right)P\left(\lambda,z\right)$$
 Eq. (2)

The equations are also valid for a pump at a wavelength  $\lambda_p$ , for which g is negative and represents the (hot) pump depletion (i.e., useful absorption as well as parasitic losses). The ground state constitutes the LLL. The parameter  $\sigma_a$  is the cross-section for ground-state absorption (GSA) of the active centers,  $\sigma_e$  and  $\sigma_{ESA}$  are the cross-sections for stimulated emission and excited-state absorption from the ULL, and  $\alpha_{BG}$  is the background loss. The sign in the differential equation depends on the propagation direction of the considered wave. Furthermore,  $n_2$  and  $n_1$  are the fractions of the active centers in the upper and lower laser level, respectively, at a certain longitudinal position. The parameter  $N_0$  is the concentration (number density) of active centers (e.g.,  $\text{Er}^{3+}$ -ions), transversally averaged over the region of the active gain medium (e.g., the core). The parameter  $\Gamma$  is an overlap factor between the transverse light distribution and the gain medium (taking account of any transverse variations in the concentration of the active medium). Specifically,

$$N_0 \Gamma(\lambda) = \int \widetilde{N}_0(x,y) \varPsi(x,y,\lambda) dx dy$$
 Eq. (3)

where x and y are transverse coordinates,  $\tilde{N}_0$  (x, y) is the transversally resolved number density of active centers, and  $\Psi$   $(x, y, \lambda)$  is the normalized transverse intensity distribution (see, e.g., Refs. [2,8,10, 27]). In case of cladding-pumping, the overlap factor for the pump is

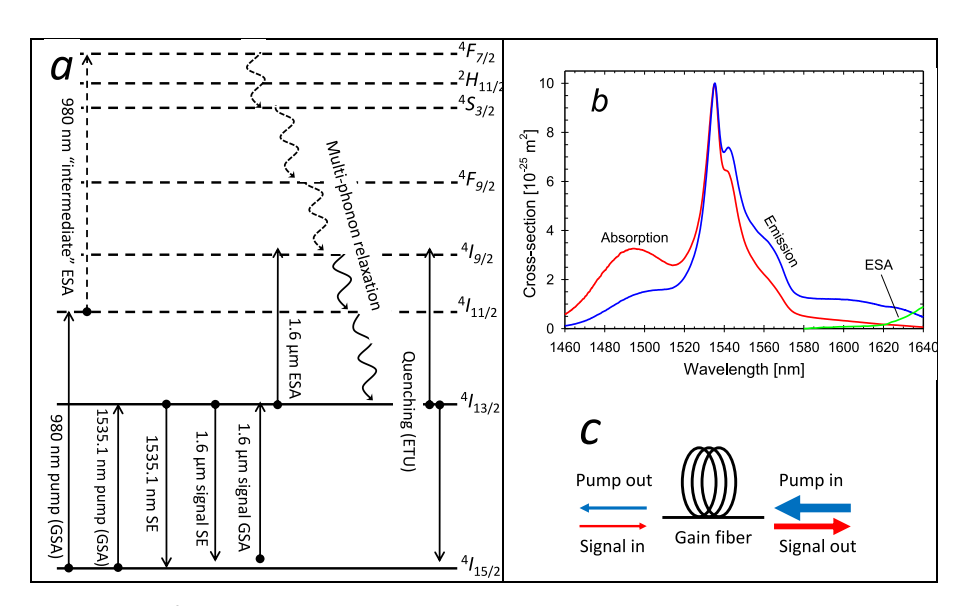


**Fig. 1.** (a) Energy levels and transitions in  $\mathrm{Er}^{3+}$ . Dashed levels and transitions are not populated or included in our modeling. The multi-phonon relaxation rate is so high that the levels affected by it are unpopulated, leaving only  ${}^4I_{13/2}$  and  ${}^4I_{15/2}$  populated. Intermediate ESA is neglected in this work but can become a factor at high power. Stark broadening is significant but is not shown. ETU: energy-transfer upconversion; SE: stimulated emission; GSA: ground-state absorption; ESA: excited-state absorption. (b) Cross-section spectra for transitions involving  ${}^4I_{13/2}$  of  $\mathrm{Er}^{3+}$  in phosphosilicate fiber. Data from Ref. [26] (room temperature). (c) Schematic of modeled configuration.

normally small and approximately equal to the inverse of the so-called (geometric) area ratio  $r_A$  between the pump waveguide (normally comprising the inner cladding and the core) and the gain medium. The overlap factor for the signal is normally much larger and can be close to unity for a core-guided signal, e.g., in case of an  $\mathrm{Er}^{3+}$ -doped fiber with homogeneous doping coincident with the core. We also introduce the effective area ratio  $r_A^{eff} = (\Gamma_s/\Gamma_p)$ . This is typically close to  $r_A$ , so typically  $r_A^{eff} >>1$  for a cladding-pumped fiber.

Typically,  $n_1$  and  $n_2$  vary along the fiber. Also  $\Gamma$  can vary along the fiber, e.g., because of different absorption of different pump modes or mode-selective gain (in case of a multimode signal). In numerical integration schemes, one can account for this by evaluating overlap integrals along the fiber, perhaps taking account of transversally resolved number densities in different energy levels. However, for our analytic treatment, we will assume that these effects are negligible so that  $\Gamma$  is constant along the fiber, thanks in part to mode-mixing effects and measures such as a well-designed inner cladding. No other parameter on the right-hand side of Eq. (1) depends on the longitudinal position in a conventional, longitudinally homogeneous fiber.

We next consider the rate equation for the excitation of the gain medium. For simplicity, we assume that only the ground state and the ULL are populated, so that  $n_1 + n_2 = 1$ . This is often appropriate for  $\mathrm{Er}^{3+}$  but is not a requirement for our analytic approach. However, if also other levels are populated and thus involved in the laser cycle then Eq. (1) needs to be modified. We also assume that there is a single pump and signal. We can then write the following rate equation for  $n_2$  [2,3,10,27].

$$dn_2 / dt = \left[\sigma_a^p \Phi_p + \sigma_a^s \Phi_s\right] n_1 - \left[\sigma_e^p \Phi_p + \sigma_e^s \Phi_s + \tau_{fl}^{-1}\right] n_2, \qquad \text{Eq. (4)}$$

where t is time,  $\Phi_p$  and  $\Phi_s$  are the pump and signal photon flux densities, and  $\tau_{\rm fl}^{-1}$  is the spontaneous relaxation rate. Furthermore, we use the shortform  $\sigma_s^a$  for the absorption cross-section at the signal wavelength  $\lambda_s$ , etc., and have dropped the explicit z-dependence. The photon flux densities have been averaged over the distributions of the active centers and intensity of the lightwaves, i.e., for the pump,

$$\Phi_p = \Gamma_p P_p / (h\nu_p A_{gm}), \qquad \text{Eq. (5)}$$

where  $P_p$  is the pump power,  $h\nu_p$  is the pump photon energy, and  $A_{gm}$  is an (effective) cross-sectional area of the active gain medium (e.g., the core area).

We will consider the steady state, i.e.,  $dn_2/dt = 0$ . With  $n_1 = (1 - n_2)$ , Eq. (4) becomes

$$0 = \left[\sigma_a^p \Phi_p + \sigma_a^s \Phi_s\right] - \left[\left(\sigma_a^p + \sigma_e^p\right) \Phi_p + \left(\sigma_a^s + \sigma_e^s\right) \Phi_s + \tau_{fl}^{-1}\right] n_2.$$
 Eq. (6)

There is no ESA in the rate equations, but this does not mean it is neglected. Rather, we assume that an active center which through ESA is further excited from the ULL to a higher-lying energy level instantaneously relaxes back to the ULL, leaving  $n_2$  unchanged. In Er $^{3+}$ , excited-state absorption can occur from  $^4I_{13/2}$  (ULL) to the level  $^4I_{9/2}$ . From there, the ion rapidly relaxes back to the ULL (via  $^4I_{11/2}$ ). In a phosphosilicate host, the relaxation time may be  $\sim 3~\mu s$  [28] or  $\sim 5.2~\mu s$  [22], although literature values vary considerably.

The treatment above is quite standard and widely used. To proceed, we will make some less common assumptions. First, we assume that  $(\sigma_p^0 + \sigma_p^0) \Phi_p + (\sigma_s^\delta + \sigma_s^\delta) \Phi_s >> \tau_{\rm fl}^{-1}$ . This is very well fulfilled in a high-power EDFA, operating in the strongly saturated regime. For example, already a signal power density of 10 mW/ $\mu$ m², which is relatively low for a high-power fiber amplifier even in the signal input end, is around two orders of magnitudes higher than the saturation intensity of the signal. Eq. (6) can then be written as

$$0 = \left[\sigma_a^p + \sigma_a^s \left(\Phi_s \middle/ \Phi_p\right)\right] - \left[\left(\sigma_a^p + \sigma_e^p\right) + \left(\sigma_a^s + \sigma_e^s\right) \left(\Phi_s \middle/ \Phi_p\right)\right] n_2, \quad \text{Eq. (7)}$$

where we have also divided by  $\Phi_p$ . Solving for  $n_2$ ,

$$n_2 = \frac{\sigma_a^p + \sigma_a^s (\Phi_s/\Phi_p)}{(\sigma_a^p + \sigma_e^p) + (\sigma_a^s + \sigma_e^s) (\Phi_s/\Phi_p)}$$
 Eq. (8)

For our purpose, a crucial feature of this solution is that the dependence of  $n_2$  on  $\Phi_s$  and  $\Phi_p$ , and thus on  $P_s$  and  $P_p$ , reduces to a dependence on the ratio  $(\Phi_s/\Phi_p)$ , and thus on the ratio  $(P_s/P_p)$ . We will refer to this as the power ratio dependence condition, PRDC, and note that this is fulfilled also when  $n_2$  is independent of  $(P_s/P_p)$ .

Eq. (8) can be used with Eq. (1) and Eq. (2) to calculate the evolution of the pump and signal power. As a crucial next step, we find a condition for which the ratio  $(P_s/P_p)$  and thus  $(\Phi_s/\Phi_p)$  are constant along the fiber. This will be the case for counter-propagating pump and signal if  $g(\lambda_s) = -g(\lambda_p)$  everywhere in the fiber. From Eq. (1) with  $n_1 = (1 - n_2)$ , this is fulfilled when  $n_2$  is given by Eq. (9).

$$n_2 = \frac{\Gamma_p \sigma_a^p + \Gamma_s \sigma_a^s + \left(\alpha_{BG}^p + \alpha_{BG}^s\right) / N_0}{\Gamma_p \left(\sigma_a^p + \sigma_e^p - \sigma_{ESA}^p\right) + \Gamma_s \left(\sigma_a^s + \sigma_e^s - \sigma_{ESA}^s\right)}$$
 Eq. (9)

If this expression is used in Eq. (1) then the signal gain will be equal to the similarly calculated pump depletion. We will refer to it as the "balanced gain" and note that this is in general only possible when there is only one signal and one pump wave.

By equating Eqs. (8) and (9), we can eliminate  $n_2$  and find an expression for constant  $(\Phi_s/\Phi_p)$  in terms of the spectroscopic cross-sections and other fiber parameters.

$$\frac{\Phi_s}{\Phi_p} = \frac{\left[\sigma_a^p \sigma_e^s - \sigma_a^s \sigma_e^p - \sigma_a^p \sigma_{ESA}^s\right] - \frac{\Gamma_p}{\Gamma_s} \sigma_a^p \sigma_{ESA}^p - \alpha_{BG}^{\text{sum}} \frac{\sigma_a^p + \sigma_e^p}{N_0 \Gamma_s}}{\frac{\Gamma_p}{\Gamma_s} \left[\sigma_a^p \sigma_e^s - \sigma_a^s \sigma_e^p + \sigma_a^s \sigma_{ESA}^p\right] + \sigma_a^s \sigma_{ESA}^s + \alpha_{BG}^{\text{sum}} \frac{\sigma_a^b + \sigma_e^s}{N_0 \Gamma_s}}$$
Eq. (10)

where  $\alpha_{BG}^{sum} = \alpha_{BG}^p + \alpha_{BG}^s$ . Here,  $\sigma_a^p$  and  $\sigma_s^e$ , and especially their product  $\sigma_a^p \times \sigma_s^e$ , are typically large relative to other analogous quantities (e.g.,  $\sigma_a^s$ ,  $\sigma_e^p$ ,  $\sigma_s^a \times \sigma_e^p$ , and, in case of Er<sup>3+</sup>,  $\sigma_{ESA}$ ). Also,  $(\Gamma_p/\Gamma_s) = (1/r_A^{eff})$  is typically small

We next introduce quenching. In  $Er^{3+}$ , this can be caused by energy transfer between neighboring ions in the ULL  ${}^4I_{13/2}$  [14–22]. One ion is then de-excited, while the other one first upconverts to  ${}^{4}I_{9/2}$  and then quasi-instantaneously relaxes back to the ULL (like for signal-ESA). Quenching can be modeled in different ways, e.g., with a shortened ULL lifetime or a relaxation term that depends nonlinearly on the fractional excitation introduced in the rate equation Eq. (4). However, neither of these two common approaches leads to solutions that fulfill the PRDC. Instead, we treat the quenching as a separate fraction  $r_0$  of active centers with a separate excitation level  $n_2^Q$ . When this also satisfies the PRDC, the overall excitation of active centers will, as well. For simplicity, we will adopt the approach that the quenched centers cannot be excited, i.e.,  $n_2^Q = 0$ . The quenched centers still absorb, and therefore add to the background loss according to the absorption cross-sections of the quenched centers  $\sigma^p_{a,Q}$  and  $\sigma^s_{a,Q}$ . Thus, the background loss increases by  $r_Q N_0 \Gamma_p \sigma^p_{a,Q}$  for the pump and  $r_Q N_0 \Gamma_s \sigma^s_{a,Q}$  for the signal. We note that  $\sigma_{a,Q}$  and hence the effect of quenching is expected to increase for shorter wavelengths within the typical signal wavelength range of 1560-1620 nm of cladding-pumped EDFAs.

We can now rewrite Eq. (10) to include quenching as follows.

$$\frac{\Phi_{s}}{\Phi_{p}} = \frac{\Gamma_{s}}{\Gamma_{p}} \frac{1 - \Gamma_{p} \sigma_{a}^{p} \frac{\Gamma_{s} \sigma_{ESA}^{s} + \Gamma_{p} \sigma_{ESA}^{p} + \left(1 + \frac{\sigma_{p}^{p}}{\sigma_{a}^{p}}\right) \frac{\sigma_{BG}^{sum}}{\rho_{a}^{p}} \frac{\Gamma_{s} \sigma_{a,Q}^{s} + \Gamma_{p} \sigma_{a,Q}^{p}}{1 - r_{Q}}}{\Gamma_{s} \Gamma_{p} \left(\sigma_{a}^{p} \sigma_{e}^{s} - \sigma_{a}^{s} \sigma_{e}^{e}\right)} }$$

$$1 + \Gamma_{s} \sigma_{a}^{s} \frac{\Gamma_{s} \sigma_{ESA}^{s} + \Gamma_{p} \sigma_{ESA}^{p} + \left(1 + \frac{\sigma_{e}^{s}}{\sigma_{a}^{p}}\right) \frac{\sigma_{BG}^{sum}}{\rho_{BG}^{s}} \frac{\Gamma_{s} \sigma_{a,Q}^{s} + \Gamma_{p} \sigma_{a,Q}^{p}}{1 - r_{Q}}}{\Gamma_{s} \Gamma_{c} \Gamma_{c} \left(\sigma_{a}^{p} \sigma_{e}^{s} - \sigma_{a}^{s} \sigma_{e}^{p}\right)} }$$
Eq. (11)

Finally, we can evaluate the PCE  $\eta$  to obtain the main result of this paper.

$$\begin{split} \eta &= \frac{P_{s}^{out} - P_{s}^{in}}{P_{p}^{in} - P_{p}^{out}} = \frac{P_{s}^{out}}{P_{p}^{in}} = \frac{\Gamma_{p}}{\Gamma_{s}} \frac{\lambda_{p}}{\lambda_{s}} \frac{\Phi_{s}}{\Phi_{p}} \\ &= \frac{\lambda_{p}}{\lambda_{s}} \frac{1 - \Gamma_{p} \sigma_{p}^{p} \frac{\Gamma_{s} \sigma_{\text{ESA}}^{s} + \Gamma_{p} \sigma_{\text{ESA}}^{p}}{\Gamma_{s} \sigma_{\text{ESA}}^{s} + \Gamma_{p} \sigma_{\text{ESA}}^{p}} \frac{\left(1 + \frac{\sigma_{p}^{p}}{\sigma_{p}^{s}}\right) \frac{\sigma_{\text{sum}}^{um} / N_{0} + r_{Q} \left(\Gamma_{s} \sigma_{a,Q}^{s} + \Gamma_{p} \sigma_{a,Q}^{p}\right)}{1 - r_{Q}}}{\Gamma_{s} \Gamma_{p} \left(\sigma_{p}^{a} \sigma_{s}^{s} - \sigma_{a}^{s} \sigma_{e}^{s}\right)} \\ &= \frac{1 + \Gamma_{s} \sigma_{s}^{a} \frac{\Gamma_{s} \sigma_{\text{ESA}}^{s} + \Gamma_{p} \sigma_{\text{ESA}}^{p} + \left(1 + \frac{\sigma_{p}^{s}}{\sigma_{p}^{s}}\right) \frac{\sigma_{\text{sum}}^{um} / N_{0} + r_{Q} \left(\Gamma_{s} \sigma_{a,Q}^{s} + \Gamma_{p} \sigma_{a,Q}^{p}\right)}{1 - r_{Q}}}{1 + \Gamma_{s} \sigma_{s}^{a} \frac{\Gamma_{s} \sigma_{\text{ESA}}^{s} + \Gamma_{p} \sigma_{\text{ESA}}^{p} + \left(1 + \frac{\sigma_{p}^{s}}{\sigma_{p}^{s}}\right) \frac{\sigma_{\text{sum}}^{um} / N_{0} + r_{Q} \left(\Gamma_{s} \sigma_{a,Q}^{s} + \Gamma_{p} \sigma_{a,Q}^{p}\right)}{1 - r_{Q}}} \end{split}$$

$$Eq. (12)$$

where superscripts *in* and *out* designate input and output powers. Also, we have used that  $(P_s/P_p)$  and  $(\Phi_s/\Phi_p)$  are constant along the fiber and have replaced  $(\Phi_s/\Phi_p)$  according to Eq. (11). The factor  $(\lambda_p/\lambda_s)$  corresponds to the difference between power conversion efficiency and quantum conversion efficiency. It is straightforward to also calculate the efficiency with respect to input pump power  $P_p^{in}$ :

$$\eta_L = \frac{P_s^{out} - P_s^{in}}{P_p^{in}} = \eta \left( 1 - G_{lin}^{-1} \right)$$
 Eq. (13)

where  $G_{lin}$  is the total linear gain in the fiber.

We note that all pump and signal cross-sections are (or can be) preceded by their respective overlap factors. Thus, the product  $\Gamma_p$   $\sigma_a^p$ , etc., can be thought of as effective cross-sections, and generally, it is possible to rewrite Eq. (12) in various ways to highlight different aspects and treat different cases. For example, with our assumption that the quenching just adds to the background loss, it is convenient to introduce  $\alpha_{BG,Q}^{SUR} = \alpha_{BG}^{SUR} + r_Q N_0 (\Gamma_p \sigma_{Q,Q}^p + \Gamma_s \sigma_{Q,Q}^s)$ . Then,

$$\eta = \frac{\lambda_{p}}{\lambda_{s}} \frac{1 - \Gamma_{p} \sigma_{p}^{p} \frac{\Gamma_{s} \sigma_{ESA}^{s} + \Gamma_{p} \sigma_{ESA}^{p}}{\Gamma_{s} \Gamma_{p} (\sigma_{a}^{p} \sigma_{e}^{s} - \sigma_{a}^{s} \sigma_{e}^{p})} \frac{\sigma_{BGQ}^{amn}}{\left(1 - \tau_{Q}\right) N_{0}}}{1 + \Gamma_{s} \sigma_{s}^{s} \frac{\Gamma_{s} \sigma_{ESA}^{s} + \Gamma_{p} \sigma_{ESA}^{p} + \left(1 + \frac{\sigma_{e}^{s}}{\sigma_{a}^{s}}\right) \frac{\sigma_{BGQ}^{amn}}{\left(1 - \tau_{Q}\right) N_{0}}}{\Gamma_{s} \Gamma_{p} (\sigma_{a}^{p} \sigma_{e}^{s} - \sigma_{a}^{s} \sigma_{e}^{p})} \right)} \\
= \frac{\lambda_{p}}{\lambda_{s}} \frac{1 - \frac{\sigma_{a}^{s} \left(\sigma_{ESA}^{s} + \frac{\rho_{ESA}^{p}}{\Gamma_{s}}\right) + \left(\sigma_{e}^{p} + \sigma_{e}^{p}\right) \frac{\sigma_{BGQ}^{amn}}{\sigma_{BGQ}^{s}}}{\sigma_{s}^{q} \sigma_{e}^{s} - \sigma_{a}^{s} \sigma_{e}^{p}}} \\
\frac{1 - \frac{\sigma_{a}^{s} \left(\sigma_{ESA}^{s} + \frac{\rho_{ESA}^{p}}{\Gamma_{s}}\right) + \left(\sigma_{e}^{q} + \sigma_{e}^{p}\right) \frac{\sigma_{BGQ}^{amn}}{\sigma_{BGQ}^{s}}}{\sigma_{s}^{q} \sigma_{e}^{s} - \sigma_{a}^{s} \sigma_{e}^{p}}} \\
\frac{1 + r^{eff}}{\sigma_{s}^{s} \left(\sigma_{ESA}^{s} + \frac{\rho_{ESA}^{p}}{\rho_{s}^{q}}\right) + \left(\sigma_{e}^{s} + \sigma_{e}^{s}\right) \frac{\sigma_{BGQ}^{amn}}{\sigma_{BGQ}^{s}}}{\sigma_{s}^{s} \left(1 - \tau_{Q}\right) N_{0}}}$$

where we have replaced  $(\Gamma_s/\Gamma_p)$  by  $r_A^{eff}$  in the second equality.

These analytic expressions are derived for a two-level system with pump- and signal-ESA, pump and signal background losses, and quenching (which adds to the pump and signal background losses) and, to the extent that the assumptions are valid, allow us to easily and quickly evaluate the PCE on a computer. However, it is still difficult to mentally examine the significance of the different parameters. To help with this, we next consider possible simplifications. In  ${\rm Er}^{3+}$ , there is no pump-ESA from the ULL ( ${}^4I_{13/2}$ ) for typical pump wavelengths (e.g., 0.98 µm, 1.48 µm, 1.53 µm). This then justifies the assumption of  $\sigma^p_{ESA}=0$ , and allows us to use a simplified version of Eq. (14) for our calculations of the efficiency of EDFAs,

$$\eta = \frac{\lambda_{p}}{\lambda_{s}} \frac{1 - \frac{\sigma_{a}^{p} \sigma_{\text{ESA}}^{s} + (\sigma_{a}^{p} + \sigma_{e}^{p}) \frac{\sigma_{BG,Q}^{m}}{r_{s}(1 - r_{Q})N_{0}}}{\sigma_{a}^{p} \sigma_{e}^{s} - \sigma_{a}^{s} \sigma_{e}^{s}} } \\
1 - \frac{r_{e}^{eff} \sigma_{e}^{s} - \sigma_{a}^{s} \sigma_{e}^{s}}{\sigma_{a}^{s} \sigma_{e}^{s} - \sigma_{a}^{s} \sigma_{e}^{s}} \\
1 + r_{A}^{eff} \frac{\sigma_{a}^{m} \sigma_{e}^{s} - \sigma_{e}^{s} \sigma_{e}^{s}}{\sigma_{e}^{p} \sigma_{e}^{s} - \sigma_{e}^{s} \sigma_{e}^{s}} \\
1 + r_{A}^{eff} \frac{\sigma_{a}^{m} \sigma_{e}^{s} - \sigma_{e}^{s} \sigma_{e}^{s}}{\sigma_{e}^{p} \sigma_{e}^{s} - \sigma_{e}^{s} \sigma_{e}^{s}} \\
1 + r_{A}^{eff} \frac{\sigma_{a}^{m} \sigma_{e}^{s} - \sigma_{e}^{s} \sigma_{e}^{s}}{\sigma_{e}^{p} \sigma_{e}^{s} - \sigma_{e}^{s} \sigma_{e}^{s}}$$
Eq. (15)

Furthermore,  $\sigma_a^s \sigma_e^p << \sigma_p^p \sigma_e^s$  in many systems (and  $\sigma_a^s \sigma_e^p < \sigma_a^p \sigma_e^s$  is a necessary condition for power transfer from pump to signal). This allows for further approximations, especially when  $\sigma_e^p = 0$  which it is in many laser systems, including  $\text{Er}^{3+}$  when pumped at 980 nm (given that the population of  ${}^4I_{11/2}$  is neglected).  $\Gamma_s = 1$  is another possible but small simplification. In four-level systems (e.g., Nd<sup>3+</sup>), the LLL may be unpopulated, whereby  $\sigma_a^s = 0$ . This readily allows for significant further

simplifications, but we will not discuss these.

In these expressions, the PCE depends only on the spectroscopy and cross-sectional geometry of the gain fiber, but not on the absolute power. The dependence on pump and signal wavelength is indirect, via the spectroscopy, or weak, via the quantum defect and waveguiding effects (overlap). The length ("balanced length") is related to the level of gain and pump depletion.

#### 3. Investigation of validity

To investigate the validity of our analysis, we compared results of Eq. (15) to simulations using numerical resolution of Eq. (6), Eq. (1), and Eq. (2) for a cladding-pumped EDFA with a single-mode core and counterpropagating pump and signal. The numerical simulations included spectrally resolved bi-directional ASE, through the addition of an ASE source term to Eq. (2). Nonlinearities such as four-wave mixing and stimulated Raman scattering were not considered. The simulations used transversally resolved distributions of the fractional excitation  $n_2$  and signal and ASE intensity distributions. The pump was transversely uniform across the pump waveguide, so mode-selective pump absorption was not considered. Since the simulations treat more effects than the analytic expression does, we consider them to be more accurate, offering a reference point ("ground truth") to which the analytic PCE can be compared. Tables 1 and 2 list default values for some parameters. Although not necessary, we assume that the absorption cross-sections of the quenched centers are the same as those of the unquenched ones.

Table 3 and Fig. 2 present results of the analytic expression Eq. (15) and of numerical simulations for pumping with 200 W at the  ${}^4I_{15/2} \rightarrow {}^4I_{13/2}$  absorption peak of 1535.1 nm. We investigated three signal wavelengths (1580, 1600, and 1620 nm) with 20 dB of balanced gain. This led to fiber lengths in the range 20–30 m as listed in Table 3, and fractional excitations  $n_2$  between 0.30 ( $\lambda_s = 1580$  nm) and 0.22 ( $\lambda_s = 1620$  nm). We note that the spontaneous decay which is neglected in Eq. (15) would correspond to a power loss of no more than 49.3 mW/m even if all  $\mathrm{Er}^{3+}$ -ions are excited. Given that less than half of the  $\mathrm{Er}^{3+}$ -ions are actually excited, the total loss to spontaneous decay was less than 1 W, which is indeed negligible at 200 W of pump power.

Although there is no explicit fiber length in Eq. (15), this follows from the 20 dB of balanced gain and the value of g from Eq. (1) (in turn dependent on the value of  $n_2$  from Eq. (9)). Similarly, there is no explicit input signal power, but it is straightforward to calculate this as the value which leads to 20 dB of balanced gain and pump depletion:

$$P_s^{in} = P_s^{out} / G_{lin}^s = \eta P_p^{in} / G_{lin}^s$$
 Eq. (16)

where  $G_{lin}^s$  is the linear signal gain (=100 in this case). Since the balanced input signal power depends on the balanced PCE, it is slightly

**Table 1** Selected fiber parameters.

F								
Quantity	Symbol	Value	Comments					
Diameter of core (=Er-doped region)		16 μm	Uniform Er-doping throughout the core					
NA of core		0.07	Cladding index $= 1.45$ , core index $1.4517$					
Cutoff wavelength		1463 nm						
Effective cladding diameter		96 µm	Only used for calculating pump overlap assuming circular cladding with transversally uniform pump distribution					
Er <sup>3+</sup> -concentration (number density)	$N_0$	$\begin{array}{l} 2.00 \; \times \\ 10^{25} \; m^{-3} \end{array}$						
Peak Er <sup>3+</sup> absorption of core-guided light		70 dB/m	1535.1 nm					
Fluorescence lifetime	$ au_{fl}$	10.5 ms						
Quenched Er <sup>3+</sup> -ion fraction	$r_Q$	0.05						

**Table 2**Selected fiber and default parameters. The cross-section values are for Er: phosphosilicate at room temperature [26].

			-			
Wavelength [nm]	$\lambda_s, \lambda_p$	980 Pump	1535.1 Pump	1580 Signal	1600 Signal	1620 Signal
Overlap	$\Gamma_s$ , $\Gamma_p$	1/36	1/36	0.795	0.790	0.784
ESA cross-section [pm <sup>2</sup> ]	$\sigma_{ESA}^{s}$ , $\sigma_{ESA}^{p}$	0	0	0	0.00724	0.0152
Stimulated- emission cross- section [pm <sup>2</sup> ]	$\sigma_e^s$ , $\sigma_e^p$	0	0.999	0.128	0.118	0.0919
Absorption cross- section [pm <sup>2</sup> ] (same for unquenched and quenched Er <sup>3+</sup> - ions)	$\sigma_{a}^{s}, \ \sigma_{a}^{p}, \ \sigma_{a,Q}^{s}, \ \sigma_{a,Q}^{s}, \ \sigma_{a,Q}^{p}, \ \sigma_{a,Q}^{p}, \ \sigma_{a,Q}^{p}$	0.254	0.997	0.0514	0.0322	0.0171
Loss from quenched Er <sup>3+</sup> - ions [dB/m]		0.0306	0.120	0.177	0.110	0.0582
Background loss [dB/m]	$\alpha_{BG}^{s}$ , $\alpha_{BG}^{p}$	0.05	0.05	0.05	0.05	0.05

Table 3 Results of analytic calculations (Eq. (15)) and numerical simulations for pumping at 1535.1 nm.

Signal wavelength [nm]	$\lambda_s$	1580	1600	1620
Input signal power for 20 dB of balanced gain	$P_s^{in}$	1.16	1.15	1.01
with 200 W of pump power [W]				
Analytic balanced net gain [dB/m]		0.760	0.905	0.877
Analytic fiber length for 20 of dB balanced gain		26.3	22.1	22.8
[m]				
Analytic PCE (Eq. (15))	η	0.580	0.575	0.506
Simulated PCE at balanced input signal power &	η	0.566	0.563	0.494
fiber length				

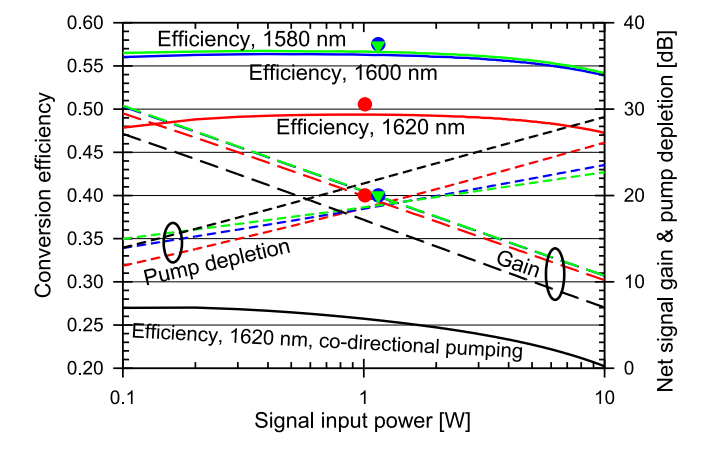


**Fig. 2.** Power conversion efficiency with respect to depleted pump power (solid curves), net signal gain (long dash), and pump depletion (short dash) for signal wavelengths of 1580 nm (green), 1600 nm (blue), and 1620 nm (red) simulated with counter-directional pump & signal. The 1580-nm (green) and 1600-nm (blue) results are close or even indistinguishable. The markers represent analytic results with 20 dB balanced signal gain & pump depletion. The black curves are for co-directional pump and 1620-nm signal. Area ratio 36 and pump wavelength 1535.1 nm. (For interpretation of the references to color in this figure legend, the reader is referred to the Web version of this article.)

different for the different signal wavelengths but becomes close to 1 W with 200 W of pump power. See Table 3.

For the simulations in Fig. 2, we used the fiber lengths calculated analytically for 20-dB balanced gain and varied the input signal power around the balanced input power in the range 0.1–10 W. Simulation results for a co-propagating pump and a signal at 1620 nm are also

included in Fig. 2. Consider first simulations with input signal power equal to the balanced value of  $\sim$ 1 W. The analytic PCEs are  $\sim$ 1% above the simulated values. The simulated signal gains are difficult to distinguish from the 20 dB of balanced gain. The deviations in pump depletion from 20 dB appear larger, but the pump leakage is anyway quite low, 1% analytically and 1.3%-1.4% in simulations, so the discrepancies in absorbed pump power are small. Thus, the agreement is good, and we expect that uncertainties in parameter values as well as modeling simplifications (e.g., in the treatment of quenching) may well lead to much larger uncertainties in the results. Nevertheless, it should be possible to reach near-perfect agreement between the analytic and simulated results when the various assumptions are well satisfied. To check if losses to spontaneous emission and ASE can explain the  $\sim 1\%$  discrepancy in PCE, we increased the pump power by ten times, to 2000 W, and the signal power by the same multiplier. This makes losses to ASE and spontaneous decay correspondingly less important. However, the agreement with Eq. (15) improved by only 0.1%. Thus, spontaneous decay and ASE cannot explain the PCE discrepancy in Fig. 2.

Another possible reason for the  $\sim \! 1\%$  discrepancy is the use of transversally resolved fractional excitations and signal and ASE intensity distributions in the numerical simulations. To assess this, we simulated a case where not only the pump but also the signal and ASE, and thus  $n_2$ , were transversely uniform. With a signal wavelength of 1620 nm and a pump power of 200 W, the PCE discrepancy becomes negligible, 0.08%. For 2000-W pumping, the discrepancy is even smaller, 0.03%. The discrepancy was negligible also with signals at 1580 and 1600 nm. This shows that Eq. (15) is highly accurate when the assumptions are well fulfilled.

By contrast, the simulated PCE with co-propagating pump and signal (1620 nm) deviates strongly from the analytic PCE, which is nearly twice as large according to Eq. (15). It is worth noting though that Fig. 2 shows the simulated results for the 22.8 m of fiber that yields 20 dB of gain analytically, according to Eq. (1) and Eq. (9). This is overlength for co-directional pumping, and with 1 W of input signal power, the PCE increases to 34.6% for a length of 16.4 m. Still, the deviation remains large, and we conclude that the analytic equations, derived for counter-directional pumping, are not valid for co-directional pumping.

The assumption that the input signal power meets the balance criterion is seldom perfectly fulfilled in practice. To investigate unbalanced conditions, we next consider the dependence of the input signal power for the counter-pumped case, plotted in Fig. 2. The pump power and fiber lengths remain as they were. The agreement between Eq. (15) and the simulations remains good or fair throughout the considered range of input signal power of 0.1-10 W (gain range around 30-10 dB). ASE remains negligible, reaching only 30 mW in the 0.1-W case and 90  $\mu$ W in the 10-W case. Overall, the agreement is worst for 10 W of input signal power, where the simulated PCE is up to 4% lower than in the balanced case. However, it is worth noting that the fiber lengths were fixed to 22-26 m (different for different signal wavelengths), corresponding to 20-dB of balanced gain. Given that the pump leakage is below -23 dBfor 10 W of input signal power, a shorter fiber with lower total background loss should increase the PCE (with respect to depleted pump power) and thus better agree with Eq. (15). We therefore simulated the dependence of the PCE on the length for 10 W of input signal power at a wavelength of 1580 nm. The PCE reached its highest value of 57.3% for a fiber length of 10.6 m. This is close to the balanced PCE of 58.0%, but we have not investigated the parameter space for which the agreement is as good as that. The signal gain was 10.0 dB (output signal power 101 W), and the pump leakage was 41.5 W (-6.83 dB). We note also that the output signal power reached its maximum of 118 W when the fiber was 22.2 m. The PCE was 54.8% and the pump leakage was -18.4 dB. The difference between fibers with length optimized for highest PCE and for highest output signal power is significant.

The unbalanced input signal power can alternatively be understood as an unbalanced fiber length. It is easy to see that the balanced linear gain and pump depletion becomes

$$G_{lin}^s = P_s^{out} / P_s^{in} = \eta P_p^{in} / P_s^{in}$$
 Eq. (17)

With 10 W of input signal power at 1580 nm and an analytic PCE of 58%, the balanced signal gain and thus the pump depletion become 10.64 dB ( $G_{lin}^{s}=11.6$ ), for a fiber length of 10.64 dB/0.760 dB/m = 14.0 m. Corresponding numerical simulations resulted in a similar PCE.

To further investigate the length dependence, we varied the length of the simulated fiber with input signal power balanced for 20 dB of gain and 200 W of pump power (thus, ~1 W of input signal power in case of ~50% PCE). Fig. 3 shows that for simulations of fibers long enough for the pump leakage to be less than -10 or -15 dB, the gain is very close to 20 dB (so the output power becomes nearly independent of fiber length), and the conversion efficiency with respect to depleted pump is close to the analytic value for the balanced case. The simulated PCE becomes much smaller than the analytic PCE in short fibers. Since the pump power is high and the signal power is low when the fiber is short, a large fraction of the unquenched Er-ions is already excited and is therefore not able to absorb the pump, so a larger fraction of the depleted pump is lost to quenched ions and background losses. Such conditions are suboptimal. A longer fiber or a higher input signal power should improve the simulated PCE. For example, the input signal power can be chosen to the value analytically balanced for a shorter fiber. At 1580 nm, the input signal power should be increased by 0.760 dB for every meter that the fiber is shorter than the balanced length of 26.3 m for the signal input power of 1.16 W used in Fig. 3.

We conclude that for these explored cases, our simple analytic expression agrees with numerical simulations for a high-power counter-directionally cladding-pumped EDFA when the parameters are reasonably well optimized. In the balanced case, the deviation in PCE from the more accurate numerical simulations was  $\sim 1\%$ , primarily caused by differences in the treatment of the transverse dependence of the signal, ASE, and fractional excitation  $n_2$ . The deviations can be larger for less appropriate parameters such as insufficient input signal power or underlength fibers. The PCE is less sensitive to excessive lengths provided that ASE remains low. Further investigations would be needed to determine the accuracy in different regimes. We also note that in no case was the simulated PCE larger than the analytic PCE. This is at least partly a consequence of the lack of losses to ASE and spontaneous emission in the analytic calculations.

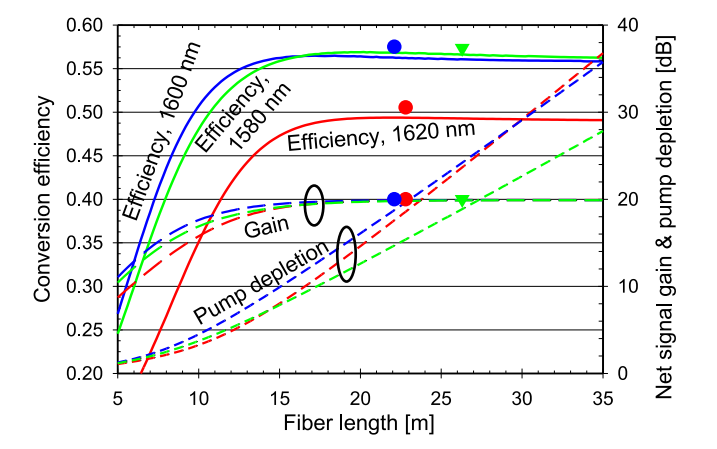


**Fig. 3.** Power conversion efficiency with respect to depleted pump power (solid curves), net signal gain (long dash), and pump depletion (short dash) for signal wavelengths of 1580 nm (green), 1600 nm (blue), and 1620 nm (red) simulated with counter-directional pump & signal. The markers represent analytic results with 20 dB balanced signal gain & pump depletion. Area ratio 36 and pump wavelength 1535.1 nm. (For interpretation of the references to color in this figure legend, the reader is referred to the Web version of this article.)

#### 4. Further results with analytic equations

We next use the analytic equations to further investigate the power conversion efficiency attainable in cladding-pumped EDFAs. First, Fig. 4 shows the PCE (Eq. (15)), fiber length, gain peak wavelength, and peak gain vs. signal wavelength for 20 dB of balanced signal gain. The gain peak wavelength and peak gain are calculated from Eq. (1) once  $n_2$  and thus  $n_1$  are determined (Eq. (9)) and the signal gain is scaled to 20 dB. The length then follows from scaling the signal gain per unit length (Eq. (1)) to 20 dB. The parameters were as previously used (see Tables 1 and 2), except that we now considered pumping at 1535.1 nm with area ratios  $r_A$  of 25, 36, 50, and 100 as well as pumping at 980 nm with  $r_A$  = 36. According to the figure, the drop in efficiency is modest when  $r_A$ increases from 25 to 50, when pumping at 1535.1 nm. For  $r_A = 36$ , pumping at 980 nm results in a PCE of 34.5%. This is significantly smaller than the 58.4% with 1535.1-nm pumping. The reduction in quantum conversion efficiency (QCE) is more modest, down to 55.6% (980-nm pumping) from 60.2% (1535.1-nm pumping). A signal wavelength of 1581 nm leads to the highest efficiency in both cases. However, some parameters in Fig. 4 lead to a peak gain that is much higher than the 20-dB balanced gain at the signal wavelength. For example,  $\lambda_p = 980$ nm,  $\lambda_s = 1581$  nm, and  $r_A = 36$  lead to a peak gain of 44.7 dB at a wavelength of 1612 nm. Such high peak gain may lead to spurious lasing as well as non-negligible levels of ASE, which are not captured by the

The high peak gain can be avoided by shifting the signal to a longer wavelength. This reduces the PCE calculated with Eq. (15) with the parameters in question, but the PCE depends only weakly on the signal wavelength in the range 1580–1615 nm, so the drop in efficiency is modest. It is also possible to reduce the balanced signal gain to, say, 15 dB, whereby the pump depletion, fiber length, and peak gain decrease in proportion. By contrast, since balancing now requires a higher input signal power, the output signal power stays the same, according to Eq. (15). Generally, precise simulations or experiments can be used to verify the analytic equations when the peak gain is high or assumptions such as negligible ASE or balanced gain are not well satisfied.

As another example, we use the analytic equations to evaluate the achievable performance vs. area ratio. This involves optimization of the PCE as follows. For each area ratio, we calculate the PCE for different signal wavelengths with 1-nm resolution and select the signal wavelength leading to the highest PCE. We then calculate other quantities as for Fig. 4. Fig. 5 shows the PCE, fiber length, signal wavelength, gain peak wavelength, and peak gain for 20 dB of balanced signal gain vs. area ratio. These quantities are plotted for different quenched ratios  $r_Q$  and pump wavelengths  $\lambda_p$ . Although the trend in Fig. 5 (a) is that a larger area ratio reduces the efficiency, it is different for small area ratios with  $r_Q=0.05$  or 0.1 and  $\lambda_p=1535.1$  nm. We attribute this to the relatively high unsaturable loss that the quenching results in for the pump, when pumping at the 1535.1-nm absorption peak with small area ratio. In such cases the efficiency may improve with pumping off the absorption peak, insofar as this also reduces the absorption of the quenched ions.

The peak gain reaches over 100 dB in Fig. 5 (c). This is unrealistic. It is however straightforward to discard signal wavelengths for which the analytic equations lead to unrealistic peak gains, for a specific area ratio. This is exemplified in Fig. 6. Similarly to Fig. 5, this shows the PCE as optimized over signal wavelength for the case of  $r_Q = 0.05$  and  $\lambda_p = 980$  nm. One set of curves is optimized over all signal wavelengths ("unrestricted peak gain") and thus repeats one of the sets in Fig. 5. The optimization for the other set of curves excludes signal wavelengths for which the peak gain exceeds 40 dB ("restricted peak gain"). Even at area ratios for which the unrestricted peak gain is much higher than 40 dB, the reduction in the efficiency resulting from the 40-dB restriction is small. The fiber lengths are also similar in the restricted and unrestricted case. By contrast, the difference in optimal signal wavelength is large. For area ratios larger than 60, the signal wavelengths become 1581 nm in the unrestricted case vs. 1612 nm in the restricted case. Note however

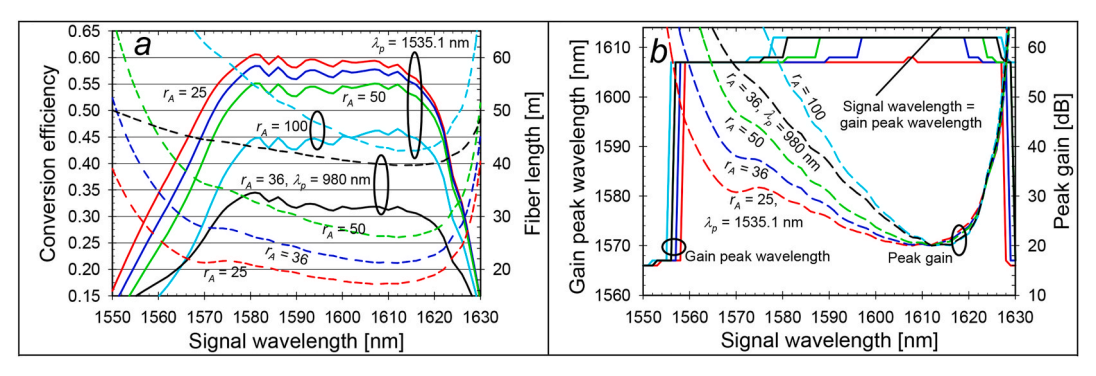


Fig. 4. (a) Power conversion efficiency  $\eta$  (solid curves) and fiber length (dashed curves) vs. signal wavelength calculated with analytic balance equations for different area ratios  $r_A$  and pump wavelengths  $\lambda_p$ . Pump wavelength 1535.1 nm with  $r_A = 25$  (red), 36 (blue), 50 (green), and 100 (cyan), and pump wavelength 980 nm with  $r_A = 36$  (black). (b) Gain peak wavelength (solid curves) and peak gain (dashed curves) with the same parameters and curve colors. Some curves overlap, making them difficult to distinguish. The signal and gain peak wavelengths coincide at the points where the solid black line "signal wavelength = gain peak wavelength" crosses the curves for the gain peak wavelength. (For interpretation of the references to color in this figure legend, the reader is referred to the Web version of this article.)

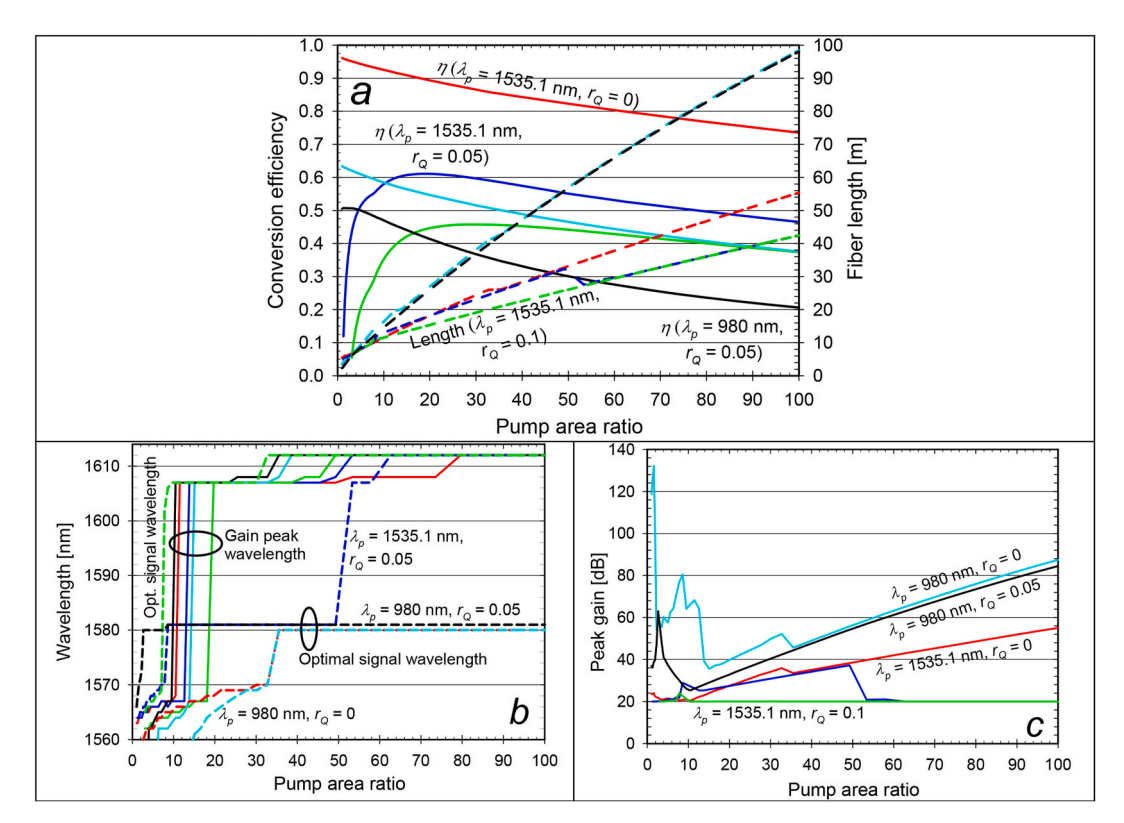


Fig. 5. (a) Power conversion efficiency  $\eta$  (solid curves) and fiber length (dashed curves) optimized over signal wavelength  $v_s$ . area ratio  $r_A$  calculated with Eq. (15) for different quenched ratios  $r_Q$  and pump wavelengths  $\lambda_p$ . Pump wavelength 1535.1 nm for  $r_Q=0$  (red),  $r_Q=0.05$  (blue), and  $r_Q=0.1$  (green). Pump wavelength 980 nm for  $r_Q=0$  (cyan) and  $r_Q=0.05$  (black). (b) Gain peak wavelength (solid curves) and optimal signal wavelength (dashed curves) with the same parameters and curve colors. (c) Peak gain with the same parameters and curve colors. Some curves overlap, making them difficult to distinguish. (For interpretation of the references to color in this figure legend, the reader is referred to the Web version of this article.)

that excessive gain can be avoided also with a signal wavelength of  $\sim\!1581$  nm, with balanced conditions (shorter fiber matched with higher signal input power) as well as unbalanced conditions (e.g., shorter fiber). This may lead to better performance than that achieved at 1612 nm with 20 dB of balanced gain.

Conventional numerical simulations can reveal additional details, e. g., how the ASE gradually becomes less significant with longer signal wavelengths, higher input signal power, or shorter fibers for parameters that may or may not match the balanced values. As an example, we used numerical simulations to investigate the impact of the high gain with  $r_A = 80$ . According to Fig. 6 (b), the optimal signal wavelength becomes

1581 nm, and the fiber length becomes 82.5 m with a balanced signal gain of 20 dB in the analytically calculated unrestricted case. The PCE  $\eta$  becomes 23.7% ( $\eta_L=23.5\%$ ) and the output signal power thus 47.4 W. The peak gain becomes 74 dB at 1612 nm. A numerical simulation leads to drastically different results, and reveals a backward ASE-power (codirectional with the pump) of 4.47 W and a forward ASE-power of 38.1 W. The signal gain becomes negative (–4.3 dB), as does the PCE. The strong ASE leads to so-called self-saturation and invalidates the analytic expressions.

We repeated the comparison for  $r_A = 80$  using the parameters of the restricted balanced case in Fig. 6. Analytically, the optimal signal

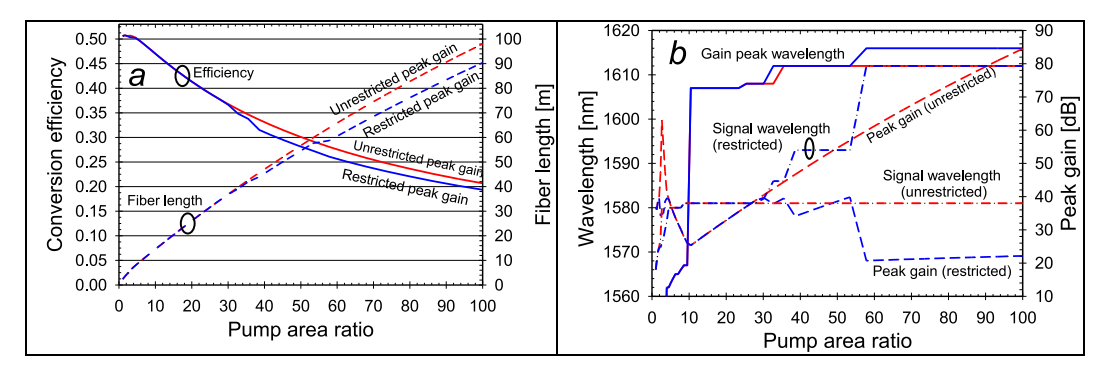


Fig. 6. (a) Power conversion efficiency  $\eta$  (solid curves) and fiber length (dashed curves) optimized over signal wavelength vs. area ratio  $r_A$  calculated with Eq. (15) for a pump wavelength of 980 nm and a quenching ratio of 0.05 with unrestricted peak gain (red curves) and peak gain restricted to  $\leq$  40 dB (blue curves). (b) Gain peak wavelength (solid curves) and optimal signal wavelength (dashed curves) for the same parameters and curve colors. (For interpretation of the references to color in this figure legend, the reader is referred to the Web version of this article.)

wavelength becomes 1612 nm and the fiber length 75.9 m for a balanced signal gain of 20 dB (Fig. 6 (b)). The PCE  $\eta$  becomes 22.1% ( $\eta_L = 21.9\%$ ) and the output signal power thus 44.2 W. The peak gain becomes 21.5 dB, at 1616 nm. A numerical simulation with the same fiber length and signal parameters lead to less than 1 mW of ASE in the forward as well as backward direction. This is negligible. The forward and backward ASE powers are now nearly the same, since the excitation level  $n_2$  is nearly constant along the fiber, close to the balanced value. The PCE becomes 21.8%, in good agreement with 22.1%.

We also compared analytic calculations and numerical simulations with unrestricted peak gain, but for a balanced signal gain of 10 dB instead of 20 dB. This reduces the balanced fiber length and the peak gain (in dB) by half. Analytically, the PCE  $\eta$  remains at 23.7% (whereas  $\eta_L$  drops to 21.3%). The numerical integration leads to a PCE of 23.4%. We attribute the good agreement to the lack of strong ASE.

# 5. Discussion

The analytic equations can be highly accurate, provided that possible sources of error such as strong ASE are kept under control. Even if the signal gain is typically not so high that it leads to significant ASE at the signal wavelength in a high-power amplifier, the peak gain may still become high enough for significant ASE as well as parasitic lasing. Therefore, the peak gain should be checked. The comparisons between the analytic calculations and simulations with balanced input signal power in conjunction with Fig. 6 illustrate this, i.e., the analytic PCE can closely approximate the numerical PCE if the peak gain is sufficiently low for ASE to be negligible. This can always be achieved by making the balanced signal gain and pump absorption sufficiently small, although it is possible that they become too small to be interesting.

A short fiber does not affect the analytic PCE  $\eta$ , since this does not depend on fiber length. However, the PCE with respect to input pump power ( $\eta_L$ ) is often more interesting, and this is reduced if the fiber is too short to adequately deplete the pump. Still, if at least 15 dB of balanced gain and pump depletion (thus 3.2% pump leakage) is realistic even without enforcing any peak gain restriction then an optimization as in Figs. 5 and 6 is expected to be valid also for  $\eta_L$  (within 3.2%, and assuming also that 15 dB of signal gain is appropriate). By contrast, the case of excessive unrestricted peak gain requires further investigations to determine how well an optimization of  $\eta_L$  with restricted peak gain (as in Fig. 6) matches numerical simulations.

The use of overlaps and transversally averaged fractional excitation is another source of error. This approximation is often used also in numerical simulations that integrate the propagation equation Eq. (2) along the fiber. We found that the differences between different cases (numerical integration without and with the use of overlaps, and the analytic calculations which use overlaps) are small. We further note that there is some freedom in the choice of the parameters  $N_0$ ,  $\Gamma$  and  $A_{gm}$  in

Eq. (3) and Eq. (5). Although there is an intuitive choice of  $N_0$  and  $A_{gm}$  (from which  $\Gamma$  follows) with our top-hat  $\mathrm{Er}^{3+}$ -distribution, it is possible that a less intuitive choice reduces the errors introduced by the overlap approach [2,8,10,27]. Deviations from the assumption that all pump modes are depleted at the same rate -g ( $\lambda_p$ ) also cause errors, but neither of these points were investigated.

Although numerical simulations can be more accurate and treat effects such as mode-selective depletion rates, the analytic approach offers several strong advantages, including analytic insight. Differentiation and other analytic manipulation are possible, too, and may allow for extensive analytic optimization, e.g., if Eq. (15) is combined with an analytic expression for the relation between number density, background loss, and quenching. However, we have not investigated if such optimization is feasible.

Computation-speed is the most obvious advantage with the analytic expressions. The numerically simulated curves in Fig. 2 (varying input signal power) and Fig. 3 (varying fiber length) are reasonably quick to evaluate, e.g., a few seconds to around a minute with an Intel i7-12850HX CPU for 100–150 samples in the curves. Although this speed may be acceptable for interactive work, the optimizations of Figs. 5 and 6 are much more computation-intensive and our numerical simulations would have taken of the order of an hour or more. By contrast, the analytic expressions actually used for those figures evaluated sufficiently rapidly for real-time updates in response to sliders controlling parameter values (overlap, quenched ion fraction, etc.) This is very helpful for the understanding of the system and the importance of different parameters in different cases. The speed of the analytic calculations also allows for multi-parameter optimization involving many millions of evaluations.

The power ratio dependence condition is conceptually crucial. Nevertheless, in Fig. 2, the analytic expression Eq. (15) was in fair agreement with numerical simulations with input signal power varying by approximately  $\pm 10$  dB from the balanced value. The power ratio ( $P_s$ /  $P_{\rm p}$ ) varied even more, by as much as  $\pm$  30 dB in Fig. 2, and still the difference between analytic and numerical calculations remains moderate. Thus, albeit conceptually crucial, the PRDC can be relatively lax in practice. One contributing factor to this is that if the input signal power is sufficiently strong to saturate the gain, the condition is automatically fulfilled near the signal output end, where most of the pump-signal conversion occurs in a counter-pumped amplifier. See Fig. 7. There, the balanced gain and pump depletion becomes 0.877 dB/m = 0.202 Np/m, so approximately  $1 - e^{-1} = 63.2\%$  of the conversion occurs within 5 m from the signal output end, in a section of the fiber where  $(P_s/P_D)$  remains reasonably close to the balanced value, despite the significant changes in input signal power.

Eq. (15) is simple to evaluate. It would be desirable to have criteria that can be evaluated easily and/or quickly, without iteration, for assessing or ensuring the validity or accuracy of the analytically calculated PCE without having to resort to comparisons to detailed numerical

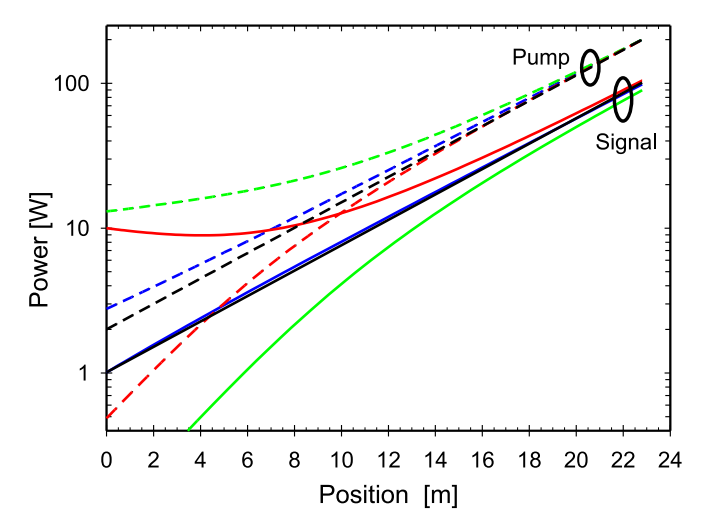


**Fig. 7.** Evolution along the fiber of pump power at 1535.1 nm (dashed curves) and signal power at 1620 nm (solid curves). Simulation results are shown for input signal powers of 0.1 W (green curves), 1.011 W (balanced case, blue), and 10 W (red). Balanced analytic results are shown, too (black curves). Other parameters are as in Tables 1 and 2 and Fig. 2. (For interpretation of the references to color in this figure legend, the reader is referred to the Web version of this article.)

simulations as in Figs. 2 and 3. We next describe such criteria, starting with the balanced case. Beyond common requirements (notably the validity of the use of constant overlap factors and negligible spurious reflections and backscatter), spontaneous emission and ASE must be negligible. The spontaneous emission was readily evaluated to less than 1 W in conjunction with Fig. 2. It is also straightforward to evaluate the peak gain, which can be used to gauge if the ASE will be small enough to not invalidate the analytic approach. This was done for Fig. 6. In borderline cases, Eq. (19) allows for a more precise, yet relatively straightforward, evaluation of the ASE and thus assessment of validity. If the ASE power is small compared to the analytically calculated output signal power, then the latter can be considered to be accurate.

Sufficiently low spontaneous emission and ASE (low peak gain or evaluated with Eq. (19)) is thus a sufficient condition for the validity of the analytic approach under balanced conditions. We also point out that

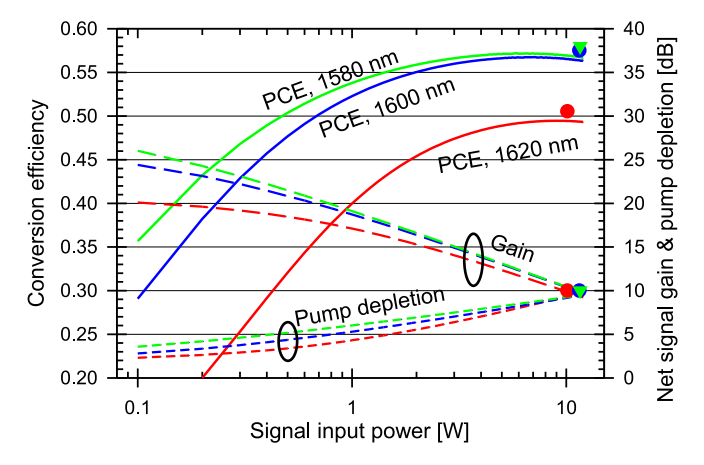


**Fig. 8.** Power conversion efficiency with respect to depleted pump power (solid curves), net signal gain (long dash), and pump depletion (short dash) for signal wavelengths of 1580 nm (green), 1600 nm (blue), and 1620 nm (red) simulated with counter-directional pump & signal. The markers represent analytic results with 10 dB balanced signal gain & pump depletion. Area ratio 36 and pump wavelength 1535.1 nm. (For interpretation of the references to color in this figure legend, the reader is referred to the Web version of this article.)

the PRDC necessarily or at least typically means that the gain is saturated under balanced conditions.

The validity of the analytically calculated PCE when applied to unbalanced cases is more difficult to assess. Above, we have discussed its accuracy in a small number of cases. Below, we provide some further examples and then outline criteria that can help to support or reject the validity of the analytic expressions in some unbalanced cases.

The balanced pump depletion of 20 dB in Fig. 2 is on the high side of normally used values. Fig. 8 repeats those calculations with a balanced depletion on the low side, namely 10 dB. Together with Fig. 2, this brackets typical depletion values. The fiber lengths become half of those for 20 dB of depletion, i.e., between 11 and 13 m. Now, Fig. 8 shows that although the analytic PCE remains a good approximation for the simulated PCE under balanced conditions ( $\sim$ 10 W of input signal power), this is no longer the case with 0.1-W of input signal power ( $\sim$ 20 dB below the balanced value). Especially at 1620 nm, the agreement is poor already 10 dB below the balanced signal input power. This contrast with Fig. 2.

To investigate these deviations further, Fig. 9 shows the PCE vs. fiber length with 0.1 W of input signal power. Fig. 9 is similar to Fig. 3, which however used input signal powers of  $\sim 1$  W, balanced for 20 dB of gain (thus slightly different input signal powers at the different wavelengths). Furthermore, the markers are now located at the balanced fiber lengths for 0.1 W and 200 W of signal and pump input powers. The balanced signal gain (same as the pump depletion) is given by Eq. (17) and becomes between 30.0 dB (1620 nm) and 30.6 dB (1600 & 1580 nm). The balanced lengths become between 34 and 40 m. With balanced lengths the simulated PCEs agree well with the analytic values. A primary reason for the poor agreement in Fig. 8 with 0.1 W of input signal power is that 10 dB of balanced pump depletion leads to severely underlength fiber (11–13 m), offering too low gain to reach saturation. Unsaturated operation is generally far from optimal and would normally be avoided, so the poor agreement may be of little consequence in practice.

ASE is another potential source of discrepancies. The drop in PCE at 1580 nm for lengths exceeding 40 m is largely a result of ASE, which peaks in the range 1605–1610 nm according to our simulations. This is caused by high gain in that wavelength range, significantly higher than the signal gain of  $\sim$ 30 dB. Indeed, from the knowledge that efficient conversion requires  $\sim$ 100 W of output signal power and thus  $\sim$ 30 dB of gain with 0.1 W of input signal power (noting also that the signal gain could never exceed 33 dB with 200 W of input pump power), it is

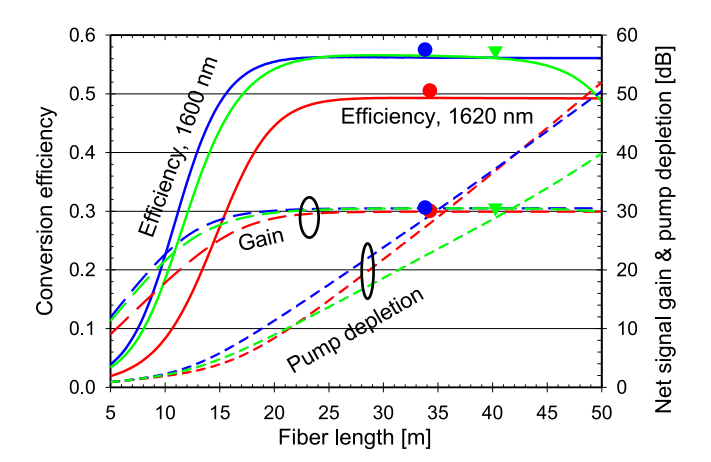


**Fig. 9.** Power conversion efficiency with respect to depleted pump power (solid curves), net signal gain (long dash), and pump depletion (short dash) for signal wavelengths of 1580 nm (green), 1600 nm (blue), and 1620 nm (red), simulated with counter-directional pump & signal. The markers represent analytic results with balanced signal gain & pump depletion for 0.1 W of input signal power at the different signal wavelengths. Area ratio 36 and pump wavelength 1535.1 nm. (For interpretation of the references to color in this figure legend, the reader is referred to the Web version of this article.)

straightforward to calculate the overall gain spectrum and peak gain from Eq. (1), scaled by the fiber length. Accordingly, we found that for a fiber length of 50 m, 30 dB of signal gain would lead to a peak gain of almost 60 dB at  $\sim\!1610$  nm. This is not realistic and would lead to parasitic emission, including ASE, as captured by the numerical simulations in Fig. 9. This example illustrates how one can check if the peak gain is excessive under unbalanced conditions, thus invalidating the analytic approach.

Unfortunately, whereas excessive peak gain is enough to cause strong ASE and thus invalidate the analytic PCE, low peak gain is not a sufficient condition for low ASE in the unbalanced case. Specifically, if the input signal power is below the balanced value, then significant ASE can arise also at wavelengths with modest or even negative total gain, due to longitudinal variations of the Er<sup>3+</sup>-excitation. See, e.g., Ref. [34]. However, if the input signal power exceeds the balanced value, then the Er<sup>3+</sup>-excitation will be below the balanced value everywhere along the fiber. It follows that also the peak gain and ASE will be below their balanced values. As a sufficient test for low ASE also in the unbalanced case, one can then verify that the balanced peak gain or ASE is sufficiently low. More precise criteria may be possible but were not investigated.

We propose that the required input signal to reach saturation can be assessed in an analogous manner, with a similar caveat about longitudinally varying excitation of the gain medium. First, using Eq. (1), calculate the excitation  $n_2$  which leads to the maximum tolerable peak gain (e.g., 40 dB). Then, calculate the signal gain for that value of  $n_2$ . If the input signal power is too low to reach the output signal power corresponding to the analytic PCE then the analytic expression will be inaccurate

In Fig. 2, also input signal powers above the balanced input signal power degrade the simulated PCE and thus the accuracy of the analytic PCE, although ASE was found to be negligible in this case. Thus, strong ASE and lack of saturation is not the only factor that causes the discrepancy (lower PCE) seen in Fig. 2. For an additional mechanism which degrades the PCE, note that in Fig. 7, the sum of the path-averaged signal and pump powers (or photon fluxes) is higher for the 0.1-W and 10-W cases than for the balanced case. This increases the losses to quenching, ESA, and background loss, thus contributing to the PCE-reduction with 0.1 W as well as with 10 W of input signal power.

Thus, we have shown that non-iterative assessment of the validity of the analytic expressions in unbalanced cases is possible. Primarily, this amounts to invalidation, whereas validation is more difficult. We expect that it will often be necessary to compare to numerical simulations to ascertain the accuracy and thus fully validate the analytically calculated PCE. This is undesirable, but it may be enough to check a small number of cases, e.g., during an optimization.

We notice that the analytically calculated PCE is larger than that of numerical simulations in all cases in Figs. 2, 3, 8 and 9. Thus, even though the analytic PCE is not always valid for unbalanced cases, a possible hypothesis is that the analytic PCE (e.g., Eq. (15)) sets an upper limit on the achievable PCE also under unbalanced conditions, and may be a good approximation for the maximum. However, this has not been verified.

We next discuss the theoretical requirements for the PRDC. First of all, this requires that there is a power ratio  $(P_s/P_p)$  such that the signal gain is equal to the operating pump depletion at their respective wavelengths. Thus, the power ratio, as well as the gain and pump depletion stay constant throughout a counter-pumped fiber amplifier even though both  $P_s$  and  $P_p$  vary. The gain and pump depletion can be a result of several types of centers, e.g., quenched and unquenched  $\operatorname{Er}^{3+}$ ions. If each of them fulfills the PRDC then also their combination will, despite their different spectroscopy. The dependence on  $(P_s/P_p)$  may well be different between the different types of centers and may well be nonlinear, e.g., in a saturating manner, or with a dependence on, e.g.,  $(P_s/P_p)^0$ ,  $(P_s/P_p)^{-0.5}$ , or  $(P_s/P_p)^2$ . In addition, the highest achievable gain must at least be as high as the smallest pump depletion  $-g(\lambda_p)$  that can be

reached. Insofar as the combined signal gain  $g(\lambda_s)$  of all types of centers decreases (i.e., saturates more strongly) monotonically and the combined pump depletion  $-g(\lambda_p)$  increases monotonically with an increase in  $(P_s/P_p)$ , there will only be one value  $(P_s/P_p)$  that fulfills the PRDC.

The requirement that the gain and pump depletion depend on the power ratio  $(P_s/P_p)$  rather than on the individual powers carries over to the level populations and has implications for the steady-state rate equations. Rate equations typically contain significant terms which are proportional to the signal photon flux density and thus the signal power, but are independent of the pump (e.g., the term  $\sigma_s^e$   $\Phi_s$  in Eq. (4)). If all significant terms are either proportional to  $\Phi_s$  or to  $\Phi_p$ , but not to both, then it is possible to divide by  $\Phi_p$  to make all significant terms proportional to either  $(P_s/P_p)^0$  or to  $(P_s/P_p)$ . If insignificant terms are neglected then the level populations (i.e., the solution to the rate equations) fulfill the PRDC. See Eq. (7) and Eq. (8), which use flux densities  $\Phi$  rather than powers.

We next discuss some rate equations different from Eq. (7). One example is the treatment of  ${\rm Er}^{3+}$  upconversion-induced concentration quenching in Ref. [18]. There, the rate equations contain a term (1 + 1/m) C  $N_2^2$  (Eq. (1) in Ref. [18]). This is significant in that it represents the quenching, but is not proportional to either  $P_s$  or  $P_p$ . Therefore, this treatment of quenching violates the PRDC.

Another treatment of quenching of  $\mathrm{Er}^{3+}$  is presented in Refs. [16,17]. This uses different rate equations for isolated (unquenched) and clustered (quenched)  $\mathrm{Er}^{3+}$ -ions. With approximations, both rate equations fulfill the PRDC, so the analytic approach presented in the current paper can be used

Another example of rate equations is provided by  ${\rm Tm}^{3+}$ -doped fiber amplifiers emitting at 2  $\mu {\rm m}$ . These benefit from a "two-for-one" cross-relaxation when pumped at 0.79  $\mu {\rm m}$  [29]. This can be modeled with a cross-relaxation term which is incompatible with the PRDC. Alternatively, however, it can be modeled simply by having each 0.79- $\mu {\rm m}$  pump photon excite a number q>1 of  ${\rm Tm}^{3+}$ -ions from the ground state  ${}^3H_6$  into the ULL  ${}^3F_4$  [30]. With this (and other) approximations, the PRDC can be fulfilled also with  ${\rm Tm}^{3+}$ -doped fiber amplifiers benefitting from "two-for-one" cross-relaxation.

The ULL lifetime is smaller in  ${\rm Tm}^{3+}$  (and  ${\rm Yb}^{3+}$ ) than in  ${\rm Er}^{3+}$ , so it may be more difficult to satisfy the assumption of negligible spontaneous decay. The analytic PCE may then agree better with the differential PCE as determined from simulations or measurements of two different combinations of balanced pump and signal powers.

We have assumed homogeneous broadening. However, our analytic approach can work also with inhomogeneous broadening, if the gain medium can be modeled with a few different types of active centers with different cross-section spectra. If each type of active centers fulfills the PRDC then we can use the approach of this paper. It is possible that also multimode amplifiers with the same gain for the different modes can be analyzed analytically.

With known background loss and a constant value of  $n_2$  along the fiber, it is in principle easy to calculate many other quantities for the balanced case. This includes the spontaneous-emission factor  $n_{sp}(\lambda)$  and the ASE spectral power density  $S_{ASE}(\lambda)$  in a single mode and polarization [W/Hz]:

$$n_{\rm sp}\left(\lambda\right) = N_0 \Gamma\left(\lambda\right) \sigma_e\left(\lambda\right) n_2 / g\left(\lambda\right)$$
 Eq. (18)

where  $n_2$  is the fractional population in the ULL and  $g(\lambda)$  [Np/m] is the gain per unit length according to Eq. (1) at some wavelength  $\lambda$ , which is in general different from the signal wavelength. See, e.g., Ref. [2]. Furthermore,

$$S_{ASE}(\lambda) = (G_{lin}(\lambda) - 1) n_{sp}(\lambda) h\nu$$
 Eq. (19)

where  $G_{lin}$  ( $\lambda$ ) is the total linear gain in the fiber and  $h\nu$  is the photon energy at the wavelength in question. The ASE power is then a spectral integral of  $S_{ASE}$ , and one can then estimate if it is large enough to affect the accuracy of the analytic equations. ASE is bi-directional and

generally different in the two directions (in which case also  $n_{sp}$  is different for the two directions). However, in the balanced case, the forward and backward ASE are equal. Note however that whereas the conversion efficiency and  $n_{sp}$  for the backward ASE are largely determined near the signal output end of the fiber,  $n_{sp}$  for the forward ASE is largely determined near the signal input. Here,  $(P_s/P_p)$  depends strongly on the input signal power (Fig. 7), and hence, so do  $n_2$  and  $n_{sp}$ . In addition, the spontaneous transition rates such as  $\tau_{fl}^{-1}$  which we neglect are more important at the signal input end. Thus, even small deviations from the ideal balanced condition can lead to differences in the forward and backward ASE.

Also the thermal load per unit length  $\dot{Q}_L(z)$  [W/m] is easy to calculate for the balanced case, if we assume that losses to scattered light are negligible. The thermal load varies along the fiber, and becomes

$$\dot{Q}_L(z) = g(\lambda_s) \left( P_p(z) - P_s(z) \right) = g(\lambda_s) P_s(z) \left( \eta^{-1} - 1 \right)$$
 Eq. (20)

This is most important in the output end.

Although generally not the case, if there are several signals or pumps at different wavelengths with the same gain or pump depletion in the gain fiber then the analytic equations can be used for all of them. This can be relevant for high-power amplifiers for wavelength-division-multiplexed signals. The relative signal powers can be chosen arbitrarily, for example, they can be equal. However, the sum of the signal powers (or photon fluxes) is not constant if the spectral distribution is changed, since the level populations must be kept at the balanced values. This also means that the PCE depends on the spectral power distribution. Furthermore, in an unlikely scenario, one can also have signals with different gain, provided that each of them is matched with a different pump and all are balanced for the same level populations. Two signals can even propagate in opposite directions, if all the pumps are counter-directional to the signal they are matched with.

In case of a counter-pumped laser in a ring-cavity, the analytic equations are directly applicable. For balancing, the pump absorption should match the signal gain in the gain fiber, and thus the signal loss in the other parts of the fiber, but as we found for the amplifier configuration, the accuracy may be reasonable even with relatively poor balancing. The output coupling must also be considered in the efficiency calculation. For a counter-pumped Fabry-Pérot (i.e., linear) laser cavity, the analytic equations may still be reasonably accurate if the intracavity laser field co-propagating with the pump (away from the output coupler) is sufficiently weak. Reference [31] presents a related analysis of the efficiency of a Fabry-Pérot laser with double-ended output. This links the measured efficiency to the background loss. Similarly, it may be possible to use also the expressions presented in this paper to deterparameters from measured mine spectroscopic efficiency characteristics.

According to our calculations, the PCE is higher for pumping at the  $^4I_{13/2}$  absorption peak (~1535.1 nm in phosphosilicate) than for pumping at the  ${}^4I_{11/2}$  absorption peak (980 nm). This is also borne out by experiments (e.g., Refs. [20-22,32,33]). On the other hand, fiber-coupled diode lasers for pumping at 980 nm are more efficient (electrical-to-optical conversion efficiency >50%) than diode lasers at ~1535 nm (electrical-to-optical conversion efficiency e.g., 24%). Also the brightness and cost are superior for 980-nm diode lasers. This can allow for smaller cladding/core area ratios, which also typically allows for higher efficiency and/or higher output power. Tandem-pumping with Er-doped fiber lasers at 1535 nm is likely to allow for the highest output power [21,22], but with the downside of low overall efficiency and high complexity. We also note also that diode lasers can be wavelength-combined to increase the brightness and power that can be launched into a given Er-doped fiber. This approach benefits from the broad absorption spectrum around 1.5 μm (including 1535.1 nm).

#### 6. Conclusions

We have derived and assessed an explicit analytic expression for the power conversion efficiency of cw optical fiber amplifiers with counterpropagating pump and signal in the presence of quenching, excited-state absorption, and background loss. The expression is simple and quick to evaluate. A crucial assumption is that the gain does not depend on the signal and pump powers separately, but rather on their ratio. This allows the signal/pump power ratio and thus the excitation level to remain constant throughout the amplifier, when the signal gain is equal to the operating pump depletion (balanced signal and pump). Typically, the assumptions can be fulfilled when each significant term in the rate equations is proportional to either the signal or the pump power, but not to both. This requires that spontaneous decay rates are negligible, or high enough to render a level population negligible.

Equations were derived specifically for an  $\mathrm{Er}^{3+}$ -doped fiber amplifier with two excited levels i.e., the upper laser level ( $^4I_{13/2}$ ) and lower laser level (the ground state  $^4I_{15/2}$ ). These are used to calculate the efficiency of cladding-pumped high-power EDFAs in phosphorus-rich erbium-doped silica fibers. We find that the analytically calculated PCE agrees well with the PCE obtained with numerical simulations using established methods in several investigated cases, some of which deviate significantly from the condition of balanced gain. However, the agreement degrades when the peak gain is so high that ASE becomes significant.

We used the equations to optimize the PCE of the EDFAs under balanced conditions, without and with a restriction on the peak gain, designed to suppress the ASE and thus ensure validity. The calculations are sufficiently fast for optimized curves to be updated real-time when parameters (e.g., for quenching) are changed. If our derived analytic expressions are combined with analytic expressions describing, e.g., cross-section spectra then this may allow for analytic optimization, although this was not investigated.

We presented non-iterative tests for the validity of the analytic equations which can be used in the balanced case. Any combination of sufficiently large input signal and pump power can be balanced by adjusting the fiber length. However, the fiber length will normally be different, leading to unbalanced operation in which the signal gain differs from the pump depletion. There are some non-iterative tests for the validity of the analytically calculated PCE also in some unbalanced cases. However, in other unbalanced cases, validity checks will require comparisons to burdensome iterative numerical simulations, although it may not be necessary to verify all analytic calculations, e.g., during an optimization.

We believe that our approach is valid for a range of realistic systems, including for example Yb-doped and Tm-doped fiber amplifiers as well as inhomogeneously broadened systems.

## Disclosures

The author declares no conflicts of interest.

All data supporting this study are openly available from the University of Southampton repository at https://doi.org/10.5258/SOTON/D3298 [35].

#### **Funding**

AFOSR (FA9550-17-1-0007).

#### **Declaration of competing interest**

I declare that I have no conflict of interest.

# Acknowledgments

Dr. Ziwei Zhai and Professor Jayanta K. Sahu provided the cross-

section spectra used in this work. Professor Sir David N. Payne is acknowledged for continuous inspiration.

#### Data availability

Data will be freely available in DOI

#### References

- A.A.M. Saleh, R.M. Jopson, J.D. Evankow, J. Aspell, Modeling of gain in erbiumdoped fiber amplifiers, IEEE Photon. Technol. Lett. 2 (1990) 714–717.
- [2] C.R. Giles, E. Desurvire, Modeling erbium-doped fiber amplifiers, J. Lightwave Technol. 9 (1991) 271–283.
- [3] B. Pedersen, A. Bjarklev, J.H. Povlsen, K. Dybdal, C.C. Larsen, The design of erbium-doped fiber amplifiers, J. Lightwave Technol. 9 (1991) 1105–1112.
- [4] Y. Sun, J.L. Zyskind, A.K. Srivastava, Average inversion level, modeling, and physics of erbium-doped fiber amplifiers, IEEE J. Sel. Top. Quant. Electron. 3 (1997) 991–1007.
- [5] M.J. Digonnet, Theory of operation of three and four-level fiber amplifiers and sources, in: M.J. Digonnet (Ed.), Fiber Laser Sources and Amplifiers, vol. 1171, Proc. SPIE, 1989, pp. 8–26.
- [6] M. Peroni, M. Tamburrini, Gain in erbium-doped fiber amplifiers: a simple analytical solution for the rate equations, Opt. Lett. 15 (1990) 842–844.
- [7] T.G. Hodgkinson, Average power analysis technique for erbium-doped fiber amplifiers, IEEE Photon. Technol. Lett. 3 (1991) 1082–1084.
- [8] T. Pfeiffer, H. Bülow, Analytical gain equations for erbium-doped fiber amplifiers including mode field profiles and dopant distribution, IEEE Photon. Technol. Lett. 4 (1992) 449–451.
- [9] T. Georges, E. Delevaque, Analytic modelling of high-gain erbium-doped fiber amplifiers, Opt. Lett. 17 (1992) 1113–1115.
- [10] C. Barnard, P. Myslinski, J. Chrostowski, M. Kavehrad, Analytical model for rareearth-doped fiber amplifiers and lasers, IEEE J. Quant. Electron. 30 (1994) 1817–1830
- [11] S. Jarabo, Analytical theoretical modeling of erbium-doped fibre amplifiers, Opt Commun. 181 (2000) 303–311.
- [12] D.J. Richardson, J. Nilsson, W.A. Clarkson, High power fiber lasers: current status and future perspectives, J. Opt. Soc. Am. B 27 (2010) B63–B92 (Invited).
- [13] J.E. Townsend, W.L. Barnes, K.P. Jedrzejewski, S.G. Grubb, Yb<sup>3+</sup> sensitised Er<sup>3+</sup> doped silica optical fiber with ultrahigh transfer efficiency and gain, Electron. Lett. 27 (1991) 1958–1959.
- [14] M. Shimizu, M. Yamada, M. Horiguchi, E. Sugita, Concentration effect on optical amplification characteristics of Er-doped silica single-mode fibers, IEEE Photon. Technol. Lett. 2 (1990) 43–45.
- [15] P. Blixt, J. Nilsson, T. Carlnäs, B. Jaskorzynska, Concentration dependent upconversion in Er<sup>3+</sup>-doped fiber amplifiers: experiments and modeling, IEEE Photon. Technol. Lett. 3 (1991) 996–998.
- [16] E. Delevaque, T. Georges, M. Monerie, P. Lamouler, J.-F. Bayon, Modeling of pair-induced quenching in erbium-doped silicate fibers, IEEE Photon. Technol. Lett. 5 (1993) 73–75.
- [17] J. Nilsson, B. Jaskorzynska, P. Blixt, Performance reduction and design modification of erbium-doped fiber amplifiers resulting from pair-induced quenching, IEEE Photon. Technol. Lett. 5 (1993) 1427–1429.

- [18] J. Nilsson, P. Blixt, B. Jaskorzynska, J. Babonas, Evaluation of parasitic upconversion mechanisms in Er-doped silica-glass fibers by analysis of fluorescence at 980 nm, J. Lightwave Technol. 13 (1995) 341–349.
- [19] V. Chernyak, Li Qian, Modeling high-concentration L-band EDFA at high optical powers based on inversion function, IEEE J. Sel. Top. Quant. Electron. 8 (2002) 569–574.
- [20] L.V. Kotov, M.E. Likhachev, M.M. Bubnov, O.I. Medvedkov, M.V. Yashkov, A. N. Guryanov, J. Lhermite, S. Février, E. Cormier, 75 W 40% efficiency single-mode all-fiber erbium-doped laser cladding pumped at 976 nm, Opt. Lett. 38 (2013) 2230–2232.
- [21] M.A. Jebali, J.-N. Maran, S. LaRochelle, 264 W output power at 1585 nm in Er-Yb codoped fiber laser using in-band pumping, Opt. Lett. 39 (2014) 3974–3977.
- [22] Guohao Fu, Guanzhong Li, Weilong Yu, Li Pei, Dan Li, Qirong Xiao, Mali Gong, Ping Yan, A 301 W narrow-linewidth in-band pumped Er:Yb co-doped fiber amplifier at 1585 nm and related modeling for dynamics study and optimization, High Power Laser Science and Engineering 12 (2024) e40.
- [23] R. Wyatt, Spectroscopy of rare-earth doped fibers, in: P.W. France (Ed.), Optical Fiber Lasers and Amplifiers, 79, CRC Press. Inc., 1991.
- [24] M. Kakui, T. Kashiwada, M. Onishi, M. Shigematsu, M. Nishimura, Optical amplification characteristics around 1.58 μm of silica-based erbium-doped fibers containing phosphorous/alumina as codopants, in: D. Baney, K. Emura, J. Wiesenfeld (Eds.), Optical Amplifiers and Their Applications, Vol. 25 of OSA Trends in Optics and Photonics Series, Optica Publishing Group, 1998 paper AB2.
- [25] M. Bolshtyansky, I. Mandelbaum, F. Pan, Signal excited-state absorption in the L-band EDFA: simulation and measurements, J. Lightwave Technol. 23 (2005) 2796–2799.
- [26] Z. Zhai, A. Halder, M. Núñez-Velázquez, J.K. Sahu, Temperature-dependent study on L-band EDFA characteristics pumped at 980 nm and 1480 nm in phosphorus and aluminum-rich erbium-doped silica fibers, J. Lightwave Technol. 40 (2022) 4819–4824.
- [27] M.A. Rebolledo, S. Jarabo, Erbium-doped silica fiber modeling with overlapping factors, Appl. Opt. 33 (1994) 5585–5593.
- [28] Vincent Kuhn, Near Diffraction Limited High-Power Narrow-Linewidth Er<sup>3+</sup>-Doped Fiber Amplifiers, Gottfried Wilhelm Leibniz Universität Hannover, 2011. PhD Thesis.
- [29] Stuart D. Jackson, Cross relaxation and energy transfer upconversion processes relevant to the functioning of 2  $\mu$ m Tm<sup>3+</sup>-doped silica fibre lasers, Opt Commun. 230 (2004) 197–203.
- [30] M. Grábner, B. Švejkarová, J. Aubrecht, P. Peterka, Analytical model of thulium-doped fiber laser pumped by two-for-one process, J. Lightwave Technol. 42 (2024) 2938–2944.
- [31] M.P. Buckthorpe, W.A. Clarkson, Simple method for determining quantum efficiency and background propagation loss in thulium-doped fibres, Appl. Phys. B 129 (2023) 142.
- [32] Jun Zhang, Viktor Fromzel, Mark Dubinskii, Resonantly cladding-pumped Yb-free Er-doped LMA fiber laser with record high power and efficiency, Opt Express 19 (2011) 5574–5578.
- [33] Huaiqin Lin, Yujun Feng, Yutong Feng, Pranabesh Barua, Jayanta K. Sahu, Johan Nilsson, 656 W Er-doped, Yb-free large-core fiber laser, Opt. Lett. 43 (2018) 3080–3083.
- [34] J. Nilsson, S.Y. Yun, S.T. Hwang, J.M. Kim, S.J. Kim, Long-wavelength erbium-doped fiber amplifier gain-enhanced by ASE end-reflectors, IEEE Photon. Technol. Lett. 10 (1998) 1551–1553.
- [35] Dataset for Explicit analytic efficiency equation for saturated counter-pumped fiber amplifiers: application to cladding-pumped erbium-doped fiber amplifiers. https://doi.org/10.5258/SOTON/D3298, 2024.